Available online at www.sciencedirect.com

ScienceDirect

Journal of the Nigerian Mathematical Society 34 (2015) 267–285

Journal of the Nigerian Mathematical Society

www.elsevier.com/locate/jnnms

Numerical solution for hydromagnetic boundary layer flow and heat transfer past a stretching surface embedded in non-Darcy porous medium with fluid-particle suspension

B.J. Gireesha[a,b,*], B. Mahanthesh[b,c], P.T. Manjunatha[d], R.S.R. Gorla[a]

[a] *Department of Mechanical Engineering, Cleveland State University, Cleveland, OH 44115, USA*
[b] *Department of Studies and Research in Mathematics, Kuvempu University, Shankaraghatta-577 451, Shimoga, Karnataka, India*
[c] *Department of Mathematics, Acharya Institute of Management and Science, Peenya, Bengaluru, India*
[d] *Department of Mathematics, Government Science College, Chitradurga, Karnataka, India*

Received 12 March 2015; received in revised form 24 July 2015; accepted 27 July 2015
Available online 21 August 2015

Abstract

This paper investigates the problem of MHD boundary layer flow and heat transfer of an electrically conducting dusty fluid over an unsteady stretching surface through a non-Darcy porous medium. The flow in porous medium is described by employing the Darcy–Forchheimer based model. The unsteadiness in the flow and temperature fields are because of time-dependent stretching velocity and surface temperature. The effect of thermal radiation, viscous dissipation and non-uniform heat source/sink are also taken into account. The pertinent time-dependent equations, governing the flow and heat transfer are reduced into a set of non-linear ordinary differential equations with the aid of suitable similarity transformations. The transformed equations are numerically integrated using fourth–fifth order Runge–Kutta–Fehlberg method. The effects of various physical parameters on the velocity and temperature profiles of both phases are analyzed through several plots. Obtained numerical results are compared and found to be in good agreement with previously published results as special cases of the present investigation. It is found that, by suspending fine dust particles in the clean fluid reduces the thermal boundary layer thickness. Therefore, the dusty fluids are preferable in engineering and scientific applications, involving cooling processes.

Keywords: Non-Darcy flow; Dusty fluid; Thermal radiation; Numerical solution; Unsteady stretching sheet; Viscous dissipation

1. Introduction

Boundary layer flow and heat transfer of a fluid over a stretching surface has attracted many researchers in the last few decades. Since, it has a wide range of applications in various fields such as polymer processing industries,

Peer review under responsibility of Nigerian Mathematical Society.
* Corresponding author at: Department of Studies and Research in Mathematics, Kuvempu University, Shankaraghatta-577 451, Shimoga, Karnataka, India. Tel.: +91 9741148002.
E-mail address: bjgireesu@rediffmail.com (B.J. Gireesha).

http://dx.doi.org/10.1016/j.jnnms.2015.07.003

Nomenclature

a, b, c	Constants
A^*, B^*	Space and temperature dependent heat generation or absorption parameters
B	Magnetic field
B_0	Magnetic field strength
c_p	Specific heat of the fluid phase (J/kg K)
c_m	Specific heat of the dust phase (J/kg K)
C_b	Form of Drag co-efficient
C_f	Skin-friction co-efficient
D	Constant
Ec	Eckert numebr
f	Dimensionless fluid phase velocity component
F	Dimensionless dust velocity component
f_0	Suction/blowing parameter
K	Stokes drag coefficient
k	Thermal conductivity of the fluid
k_0	Porous parameter
kp	Permeability of porous medium of variable kind
k^+	Mean absorption coefficient
${k_0}^*$	Permeability of porous medium
l	Parameter of Mass concentration of dust particles
m	Mass of dust particles
M^2	Magnetic parameter
N	Number density of dust particles
Nu	Nusselt number
Pr	Prandtl number
q_r	Radiative heat flux
q_w	Surface heat flux
q_f	Rate of heat transfer
q'''	Space and temperature dependent heat generation/absorption
R	Radiation parameter
r	Radius of dust particles
Re_x	Local Reynolds number
S	Unsteady parameter
t	Time
T	Fluid phase temperature (K)
T_p	Dust phase temperature (K)
T_w	Temperature at the wall (K)
T_∞	Ambient Temperature (K)
u, v	Fluid phase velocity components along x and y directions (m s^{-1})
u_p, v_p	Dust phase velocity components along x and y directions (m s^{-1})
U_w	Stretching sheet velocity (m s^{-1})
V_w	Suction/injection velocity (m s^{-1})
x, y	Co-ordinates (m)
ρ	Density of the fluid phase (kg/m^3)
ρ_p	Density of the dust phase (kg/m^3)
μ	Dynamic viscosity (kg m^{-1} s^{-1})
σ	Electrical conductivity of the fluid
φ	Porosity of the porous medium
ν	Kinematic viscosity of the fluid (m^2 s^{-1})

τ_v	Relaxation time of the dust particles
β_v	Fluid particle interaction parameter for velocity
α	Local inertia coefficient parameter
τ_w	Surface shear stress
τ_T	Thermal equilibrium time
σ^*	Stefan–Boltzmann constant
θ	Dimensionless fluid phase temperature (K)
θ_p	Dimensionless dust phase temperature (K)
γ	Specific heat ratio
β_T	Fluid–particle interaction parameter for temperature
η	Similarity variable

particularly, in the manufacturing process of artificial films, artificial fibers and dilute polymer solutions. In particular, it may be pointed out that many metallurgical processes involve the cooling of continuous strips or filaments by drawing them through a quiescent fluid and in the process of drawing, these strips are sometimes stretched. The heat transfer analysis over a stretching surface is of much practical interest due to its abundant applications such as heat-treated materials traveling between a feed roll and wind-up roll or materials manufactured by extrusion, glass, fiber, paper production, cooling of metallic sheets or electronic chips, drawing of plastic films and liquid films in condensation processes. In view of these applications, Sakiadis [1] initiated the study of boundary layer flow over a stretched surface moving with a constant velocity and formulated a boundary layer equation for two-dimensional and axisymmetric flows. Tsou et al. [2] analyzed the effect of heat transfer in the boundary layer on a continuous moving surface with a constant velocity and experimentally confirmed the numerical results of [1]. Later on, the heat transfer characteristics of a continuous stretching surface with variable temperature has been investigated by Grubka and Bobba [3]. Very recently, Akbar et al. [4] studied the flow of CNT suspended nanofluid over a stretching sheet.

Transport processes through porous media play an important role in many applications, such as geothermal operations, petroleum industries, thermal insulation, design of solid-matrix heat exchangers, chemical catalytic reactors, and many others. An excellent literature review on flow through porous media can be found from Starov and Zhdanov [5], Kiwan and Ali [6], Gireesha et al. [7] and Tamayol et al. [8]. Mentioned studies were based on the Darcy law to incorporate the porous medium. But in many practical situations the porous medium has huge flow rates and reveals the irregular porosity distribution near the wall region, cause inapplicability of Darcy's law. Due to this reason it is necessary to include the non-Darcian effects in the analysis of flow and heat transfer through a porous medium. Representative studies dealing with the non-Darcy porous medium effects have been reported by Hong et al. [9], Mohammadein et al. [10], Khani et al. [11] and Dulal and Chatterjee [12].

Mention can be made that, all the above said investigations are in a steady state condition. But in certain circumstances, flow become time-dependent and as a result, it is necessary to include unsteady state. Chen [13] studied the flow and heat transfer over an unsteady stretching surface in power-law fluid. Ishak et al. [14,15] obtained the numerical solution for flow and heat transfer on an unsteady stretching surface/stagnation point. Flow and heat transfer in a liquid film over an unsteady stretching surface with viscous dissipation in the presence of external magnetic field have been investigated by Abel et al. [16]. Recently, Aziz [17] analyzed mixed convection flow of a micropolar fluid from an unsteady stretching surface with viscous dissipation. The effect of viscous dissipation is foreseeable in the case of the flow field is of extreme size or in high gravitational force. In addition to this, radiative heat transfer flow is very important in manufacturing industries for the design of reliable equipments, nuclear plants, gas turbines and various propulsion devices for aircraft, missiles, satellites and space vehicles. Because of these reasons, Dulal and Mondal [18] studied the combined effects of thermal radiation and viscous dissipation on MHD non-Darcy flow and heat transfer over a stretching sheet. Cortell [19] analyzed the influence of viscous dissipation and thermal radiation on fluid flows over a non-linearly stretched permeable wall. Motsumi and Makinde [20] have presented the nanofluid boundary layer flow and heat transfer over a permeable moving flat plate with thermal radiation and viscous dissipation effects. The effects of thermal radiation on a steady MHD two dimensional stagnation point flow of an incompressible nano fluid towards a stretching cylinder has been studied by Akbar et al. [21]. Later, Mahantesh et al. [22] studied the heat transfer characteristics of viscoelastic fluid in a porous medium over a stretching sheet with viscous dissipation. Very

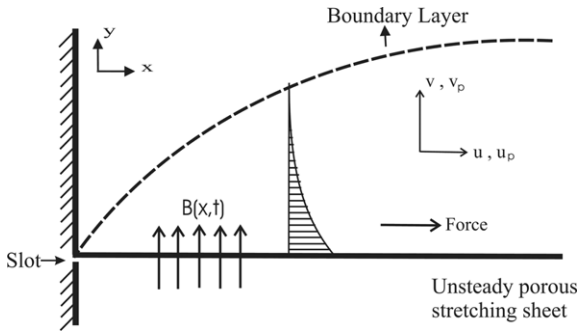

Fig. 1. Physical model and coordinate system of the problem.

recently, Liu et al. [23] investigated the effect of viscous dissipation and thermal radiation on flow and heat transfer in a hydromagnetic liquid film over an unsteady stretching sheet with the prescribed heat flux condition.

On the other hand, study of boundary layer flow and heat transfer in dusty fluid is very constructive in understanding of various industrial and engineering problems concerned with powder technology, rain erosion in guided missiles, sedimentation, atmospheric fallout, combustion, fluidization, electrostatic precipitation of dust, nuclear reactor cooling, waste water treatment, acoustics batch settling, aerosol and paint spraying, luner ash flows and etc. In view of these applications, Saffman [24] initiated the study of dusty fluids and investigated the stability of laminar flow of a dusty gas and the flow is considered to be a two-phase flow with the concept that the dust particles form a pseudofluid. Datta and Mishra [25] have analyzed the dusty fluid in boundary layer flow over a semi infinite flat plate. Later, Vajravelu and Nayfeh [26] considered the hydromagnetic flow and heat transfer of a dusty fluid over stretching sheet with suction effect. Unsteady flow and heat transfer of dusty fluid between two parallel plates with variable viscosity and thermal conductivity has been investigated by Makinde and Chinyoka [27]. Nandkeolyar et al. [28] addressed the hydromagnetic natural convection flow of a dusty fluid past an impulsively moving vertical plate with ramped temperature in the presence of thermal radiation. Recently, the boundary layer flow and heat transfer over a dusty fluid steady/unsteady stretching sheet with various aspects have been numerically investigated by Gireesha et al. [29–32].

Keeping all these facts in our mind, an attempt has been made to analyze the effects of applied transverse magnetic field, non-Darcy porous medium, suction/injection, thermal radiation, viscous dissipation and irregular internal heat source/sink on the boundary layer two-phase flow and heat transport of dusty fluid over an unsteady stretching surface. Here, two types of heating processes, namely variable wall temperature and variable heat flux are considered. The governing nonlinear partial differential equations are transformed to a set of nonlinear ordinary differential equations and then they are solved numerically by fourth–fifth order Runge–Kutta–Fehlberg scheme. The effects of various important parameters affecting the flow fields are studied by means of graphs and tables.

2. Mathematical formulation

Consider an unsteady two-dimensional laminar boundary layer flow and heat transfer of an incompressible dusty viscous fluid over a stretching sheet through a non-Darcy porous medium. The x-axis is taken along stretching surface in the direction of motion with a slot as origin, and y-axis is perpendicular to the sheet in an outward direction towards the fluid. The flow is assumed to be confined in a region of $y > 0$ as shown in Fig. 1. The flow is caused by the stretching of the sheet which moves in its own plane with the surface velocity $U_w(x,t) = bx/(1-ct)$, where b and c are positive constants with dimension reciprocal time. Here, b is the initial stretching rate, whereas the effective stretching rate $b/(1-ct)$ is increasing with time. In the context of polymer extrusion, the material properties and in particular the elasticity of an extruded sheet varies with time, even though the sheet is being pulled by a constant force. With unsteady stretching (i.e., $c \neq 0$), however, c^{-1} becomes the representative time scale of the resulting unsteady boundary layer problem. It is considered that the wall temperature $T_w(x,t)$ of the sheet is suddenly raised from T_∞ to $T_w(x,t)$ ($T_w(x,t) > T_\infty$), or there is a suddenly imposed heat flux $q_f(x,t)$ at the wall.

The dust particles are suspended in a viscous fluid using either surfactant or surface charge technology. The number density of dust particles is assumed to be constant throughout the motion and the volume fraction of the dust particles is neglected. The buoyancy forces on dust particles and inter particle reactions are neglected. In addition, the applied

transverse magnetic field and permeability of porous medium are assumed to be of variable kind and are chosen in its special form as $B = B_0/\sqrt{(1-ct)}$ and $kp = k_0{}^*(1-ct)$. It is assumed that the fluid is electrically conducting and the magnetic Reynolds number is small, so that induced magnetic field is neglected. Further, it is assumed that the effect of Hall current and Joule heating are neglected.

Under these assumptions along with the boundary layer approximations, the governing unsteady boundary layer equations of both fluid and particle phase takes the following form (see [27,28])

$$\frac{\partial u}{\partial x} + \frac{\partial v}{\partial y} = 0, \tag{2.1}$$

$$\rho\left(\frac{\partial u}{\partial t} + u\frac{\partial u}{\partial x} + v\frac{\partial u}{\partial y}\right) = \mu\frac{\partial^2 u}{\partial y^2} + KN(u_p - u) - \sigma B^2 u - \frac{\mu\varphi}{kp}u - \frac{C_b\varphi}{\sqrt{kp}}u^2, \tag{2.2}$$

$$\frac{\partial u_p}{\partial x} + \frac{\partial v_p}{\partial y} = 0, \tag{2.3}$$

$$\rho_p\left(\frac{\partial u_p}{\partial t} + u_p\frac{\partial u_p}{\partial x} + v_p\frac{\partial u_p}{\partial y}\right) = KN(u - u_p), \tag{2.4}$$

where (u, u_p) and (v, v_p) are the velocity components in x and y directions of the fluid and dust particle phase respectively. ρ is the density of the fluid, $\rho_p = mN$ is density of the dust particles, m and N are respectively, mass and number density of the dust particles per unit volume, σ is electrical conductivity of the fluid, μ is the dynamic viscosity of the fluid, φ is porosity of the porous medium, C_b is the form of drag coefficient, which is independent of viscosity and other physical properties of the fluid, which depend on the geometry of the medium, $k_0{}^*$ permeability of the porous medium, $K = 6\pi\mu r$ is the Stokes drag coefficient, r is the radius of dust particle and t is the time.

The relevant boundary conditions applicable to the present problem are

$$\begin{aligned} &u = U_w(x,t), \qquad v = V_w(x,t) \quad \text{at } y = 0,\\ &u \to 0, \qquad u_p \to 0, \qquad v_p \to v \quad \text{as } y \to \infty, \end{aligned} \tag{2.5}$$

where V_w is suction/injction velocity. It should be noted, the $(V_w < 0)$ corresponds to blowing, $(V_w > 0)$ corresponds to suction and if $(V_w = 0)$ then the stretching surface is impermeable.

Eqs. (2.1)–(2.4) subjected to boundary conditions (2.5) admits self-similar solution in terms of the similarity function f, F and similarity variable η and they are defined as;

$$\begin{aligned} &u = \frac{bx}{(1-ct)}f'(\eta), \qquad v = -\sqrt{\frac{b\nu}{(1-ct)}}f(\eta), \qquad \eta = \sqrt{\frac{U_w(x,t)}{\nu x}}y,\\ &u_p = \frac{bx}{(1-ct)}F'(\eta), \qquad v_p = -\sqrt{\frac{b\nu}{(1-ct)}}F(\eta), \end{aligned} \tag{2.6}$$

where a prime denotes the differentiation with respect to η. The Eqs. (2.1) and (2.3) are identically satisfied, in terms of relations (2.6). In addition, Eqs. (2.2) and (2.4) are reduces to the following set of non-linear ordinary differential equations;

$$\begin{aligned} &f'''(\eta) + f''(\eta)f(\eta) - (1+\alpha)f'(\eta)^2 - S\left(\frac{\eta}{2}f''(\eta) + f'(\eta)\right) + l\beta_v\left(F'(\eta) - f'(\eta)\right)\\ &\quad - \left(M^2 + k_0\right)f'(\eta) = 0, \end{aligned} \tag{2.7}$$

$$F''(\eta)F(\eta) - F'(\eta)^2 - S\left(\frac{\eta}{2}F''(\eta) + F'(\eta)\right) + \beta_v\left(f'(\eta) - F'(\eta)\right) = 0, \tag{2.8}$$

where $l = mN/\rho$ is dust particles mass concentration parameter, $\tau_v = m/K$ is relaxation time of the dust particles, $\beta_v = (1-ct)/b\tau_v$ is local fluid–particle interaction parameter, $S = c/b$ is unsteady parameter, $k_0 = \nu\varphi/k_0{}^*b$ is porous parameter, $\alpha = C_b\varphi U_w\sqrt{(1-ct)}/b\sqrt{k_0{}^*}$ is local inertia coefficient parameter and $M^2 = \sigma {B_0}^2/b\rho$ is magnetic parameter.

Substituting the Eq. (2.6) in to the boundary conditions (2.5), one can get;

$$\begin{aligned} &f'(\eta) = 1, \qquad f(\eta) = f_0 \quad \text{at } \eta = 0, \\ &f'(\eta) \to 0, \qquad F'(\eta) \to 0, \qquad F(\eta) \to f(\eta) \quad \text{as } \eta \to \infty, \end{aligned} \tag{2.9}$$

where $f_0 = V_w(x,t)/\sqrt{\nu b}$ is the suction/blowing parameter.

From the engineering point of view, the most important characteristics of the flow are the local skin-friction coefficient C_f and is given by,

$$C_f = \frac{\tau_w}{\rho {U_w}^2 \frac{1}{2}}, \tag{2.10}$$

where τ_w is the surface shear stress, which is given by

$$\tau_w = \mu \left(\frac{\partial u}{\partial y}\right)_{y=0}. \tag{2.11}$$

Using Eq. (2.11) and with the aid of similarity variables, we obtain

$$Re_x{}^{\frac{1}{2}} C_f = f''(0), \tag{2.12}$$

where $Re_x = U_w x/\nu$ is the local Reynolds number.

It is worth to mention that, if $l = f_0 = 0$, then the problem reduces to an ordinary viscous fluid flow, i.e., classical Blasius flat-plate problem. Moreover, the present investigation reduces to steady-state flow for $c = 0$. If $\alpha = k_0 = M^2 = f_0 = S = 0$, the Eq. (2.7) has the closed-form solution

$$f(\eta) = (1 - e^{-\eta}). \tag{2.13}$$

In view of the Eq. (2.13), the local skin friction co-efficient is given by

$$f''(0) = -1. \tag{2.14}$$

3. Heat transfer analysis

The governing unsteady boundary layer heat transport equations for dusty fluid with thermal conductivity, viscous dissipation, thermal radiation and non-uniform heat source/sink are given by [24];

$$\rho c_p \left(\frac{\partial T}{\partial t} + u\frac{\partial T}{\partial x} + v\frac{\partial T}{\partial y}\right) = k\frac{\partial^2 T}{\partial y^2} + \frac{\rho_p c_p}{\tau_T}(T_p - T) + \frac{\rho_p}{\tau_v}(u_p - u)^2 + \mu\left(\frac{\partial u}{\partial y}\right)^2 - \frac{\partial q_r}{\partial y} + q''', \tag{3.1}$$

$$\rho_p c_m \left(\frac{\partial T_p}{\partial t} + u_p\frac{\partial T_p}{\partial x} + v_p\frac{\partial T_p}{\partial y}\right) = -\frac{\rho_p c_p}{\tau_T}(T_p - T), \tag{3.2}$$

where T and T_p are the temperature of the fluid and dust particles respectively, c_p and c_m are the specific heat of fluid and dust particles respectively, τ_T is the thermal equilibrium time i.e., the time required by the dust cloud to adjust its temperature to that of fluid, τ_v is the relaxation time of the dust particle i.e., the time required by a dust particle to adjust its velocity relative to the fluid, k is fluid thermal conductivity and q''' is the space and temperature dependent heat generation/absorption, which can be expressed as [29];

$$q''' = \frac{kU_w(x,t)}{x\nu}\left[A^*(T_w - T_\infty)f'(\eta) + B^*(T - T_\infty)\right], \tag{3.3}$$

where A^* and B^* are parameters of space and temperature dependent heat generation or absorption respectively. It is to be noted that $A^* > 0$ and $B^* > 0$ correspond to internal heat generation, whereas $A^* < 0$ and $B^* < 0$ correspond to internal heat absorption.

The radiative heat flux q_r is employed according to the Rosseland diffusion approximation for radiation such that;

$$q_r = -\frac{4\sigma^*}{3k^+}\frac{\partial T^4}{\partial y}, \tag{3.4}$$

where σ^* is the Stefan–Boltzmann constant and k^+ is the mean absorption coefficient. It is noted that the optically thick radiation limit is considered in this model. Assuming that the temperature differences within the flow are sufficiently small such that T^4 may be expressed as a linear function of temperature, we expand T^4 in a Taylor series about T_∞ as follows,

$$T^4 = {T_\infty}^4 + 4{T_\infty}^3(T - T_\infty) + 6{T_\infty}^2(T - T_\infty)^2 + \cdot. \tag{3.5}$$

Neglect the higher order terms beyond the first degree in $(T - T_\infty)$, one can we get;

$$T^4 \cong 4{T_\infty}^3 T - 3{T_\infty}^4. \tag{3.6}$$

Substituting Eq. (3.6) in Eq. (3.4) one can get

$$\frac{\partial q_r}{\partial y} = -\frac{16{T_\infty}^4\sigma^*}{3k^*}\frac{\partial^2 T}{\partial y^2}. \tag{3.7}$$

In view of the Eq. (3.7), the energy equation (3.1) becomes

$$\rho c_p\left(\frac{\partial T}{\partial t} + u\frac{\partial T}{\partial x} + v\frac{\partial T}{\partial y}\right) = \left(k + \frac{16{T_\infty}^4\sigma^*}{3k^+}\right)\frac{\partial^2 T}{\partial y^2} + \frac{\rho_p c_p}{\tau_T}(T_p - T) + \frac{\rho_p}{\tau_v}(u_p - u)^2 + \mu\left(\frac{\partial u}{\partial y}\right)^2 + q'''. \tag{3.8}$$

The thermal boundary conditions depend on the type of heating process under consideration. In the present investigation, the heat transfer analysis has been carried out for two different heating processes namely VWT and VHF cases. To solve the Eqs. (3.8) and (3.2), the variable wall temperature and variable heat flux boundary conditions are read as

$$\begin{aligned} &T = T_w(x,t) = T_\infty + \frac{bx}{(1-ct)} \quad \text{at } y = 0, \text{ (VWT case)} \\ &-k\frac{\partial T}{\partial y} = q_f(x,t) = T_\infty + \frac{Dx}{(1-ct)} \quad \text{at } y = 0, \text{ (VHF case)} \\ &T \to T_\infty \qquad T_p \to T_\infty, \quad \text{as } y \to \infty, \end{aligned} \tag{3.9}$$

where $q_f = Dx/(1-ct)$ is the rate of heat transfer, b and D are positive constants. Now define the non-dimensional fluid phase temperature $\theta(\eta)$ and dust particle phase temperature $\theta_p(\eta)$ as

$$\theta(\eta) = \frac{T - T_\infty}{T_w - T_\infty}, \qquad \theta_p(\eta) = \frac{T_p - T_\infty}{T_w - T_\infty}, \tag{3.10}$$

where $T = \frac{bx}{(1-ct)}\theta(\eta) + T_\infty$ (VWT case), $T = T_\infty + \frac{Dx}{k(1-ct)}\sqrt{\frac{v}{b}}\theta(\eta)$ (VHF case), T_w and T_∞ denotes the temperature at the wall and at large distance from the wall respectively.

Substituting Eq. (3.10) into (3.8) and (3.2), we obtain the following set of non-linear ordinary differential equations;

$$\left(1 + \frac{4}{3}R\right)\theta''(\eta) + Pr\left(\theta'(\eta)f(\eta) - f'(\eta)\theta(\eta)\right) - S\,Pr\left(\frac{\eta}{2}\theta'(\eta) + \theta(\eta)\right) + l\,Pr\beta_T\left(\theta_p(\eta) - \theta(\eta)\right) + l\,Ec\,Pr\beta_v\left(F'(\eta) - f'(\eta)\right)^2 + Ec\,Pr\left(f''(\eta)\right)^2 + A^* f'(\eta) + B^*\theta(\eta) = 0, \tag{3.11}$$

$$\theta_p'(\eta)F(\eta) - F'(\eta)\theta_p(\eta) - S\,Pr\left(\frac{\eta}{2}\theta_p'(\eta) + \theta_p(\eta)\right) - \beta_T\gamma\left(\theta_p(\eta) - \theta(\eta)\right) = 0, \tag{3.12}$$

where $Pr = \mu c_p/k$ is the Prandtl number, $\gamma = c_p/c_m$ is specific heat ratio, $\beta_T = (1-ct)/b\tau_T$ is fluid–particle interaction parameter for temperature, $R = 4\sigma^*{T_\infty}^3/k^+k$ is the thermal radiation parameter, $Ec = {U_w}^2/c_p(T_w - T_\infty)$ (VWT) and $Ec = {U_w}^2 b^{3/2}k/Dc_p\nu^{1/2}(T_w - T_\infty)$ (VHF) are the Eckert number.

Boundary conditions (3.9) in terms of (3.10) can be written as:

$$\begin{aligned} &\theta(\eta) = 1 \quad \text{at } \eta = 0, \text{ (VWT case)} \\ &\theta'(\eta) = -1 \quad \text{at } \eta = 0, \text{ (VHF case)} \\ &\theta(\eta) \to 0, \qquad \theta_p(\eta) \to 0 \quad \text{as } \eta \to \infty. \end{aligned} \tag{3.13}$$

The important physical parameter Nusselt number is given by

$$Nu = \frac{q_w}{k(T_w - T_\infty)}, \tag{3.14}$$

where q_w is the surface heat flux, which is given by

$$q_w = -k\left(\frac{\partial T}{\partial y}\right)_{y=0}. \tag{3.15}$$

In terms of similarity variables and with the aid of Eq. (3.15), we obtain

$$Re_x^{-\frac{1}{2}} Nu = -\theta'(0). \tag{3.16}$$

It is worth to mention that, in terms of Kummers functions, the solution of the Eq. (3.11) for the case $A^* = B^* = R = Ec = S = f_0 = 0$ is given by [17]

$$\theta(\eta) = \frac{M\left(2,\ Pr+1,\ Pre^{-\eta}\right)}{M\left(2, Pr+1, Pr\right)} e^{(1-\eta-e^{-\eta})Pr}, \tag{3.17}$$

where $M(a, b, z)$ denotes the confluent hypergeometric function [33] as follows:

$$M(a, b, z) = 1 + \sum_{n=1}^{\infty} \frac{a_n z^n}{b_n n!}, \tag{3.18}$$

where

$$\begin{aligned} a_n &= a(a+1)(a+2)(a+3)\cdots, \\ b_n &= b(b+1)(b+2)(b+3)\cdots. \end{aligned}$$

In view of the Eq. (3.17), the local Nusselt number $-\theta'(0)$ is given by [17]

$$-\theta'(0) = \frac{2\,Pr}{Pr+1} \frac{M(3, Pr+2, Pr)}{M(2, Pr+1, Pr)}. \tag{3.19}$$

4. Numerical method and validation

The set of non-linear differential equations (2.7), (2.8), (3.11) and (3.12) with the boundary conditions (2.9) and (3.13) constitute a two-point boundary value problem. Due to high non-linearity nature of the equations, they are not amenable to closed form solutions, therefore we resorted to numerical solution. In order to solve these equations numerically we follow most efficient fourth–fifth order Runge–Kutta–Fehlberg integration scheme with the help of algebraic package Maple. This algorithm in Maple has been well tested for its accuracy and robustness. In this method, it is most important to choose the appropriate finite values of η_∞. The asymptotic boundary conditions at η_∞ were replaced by those at η_5 in accordance with standard practice in the boundary layer analysis. The inner iteration is counted until nonlinear solution converges with a convergence criterion of 10^{-6}. In addition, the step size is chosen as $\Delta\eta = 0.001$. In Maple package there are two submethods are available namely, trapezoidal and midpoint method. We chosen midpoint method as sub-method, since the midpoint method is so capable of handling harmless end-point singularities.

In order to validate and verify the accuracy of the applied numerical scheme, results of $-\theta'(0)$ for various values of Pr in the case of $A^* = B^* = Ec = S = f_0 = R = l = 0$ are compared with those reported by Grubka and

Table 1
Comparison results for local Nusselt number $-\theta'(0)$ in the case of $A^* = B^* = Ec = S = f_0 = R = 0$ for ordinary viscous fluid.

Pr	Grubka et al. [3]	Ishak et al. [14]	El-Aziz [17]	Exact solution [15]	Present study
0.72	0.8086	0.8086	0.80873	0.80863	0.80863
1.0	1.0000	1.0000	1.00000	1.00000	1.00000
3.0	1.9237	1.9237	1.92368	1.92368	1.92367
10.0	3.7207	3.7207	3.72067	3.72067	3.72067
100	12.294	12.2941	12.29408	12.29408	12.29408

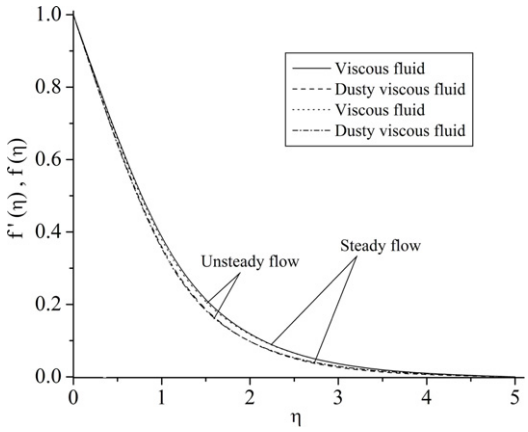

Fig. 2. Velocity of different fluids.

Bobba [3], El-Aziz [17], Ishak et al. [14] and exact solution reported in [15]. The comparisons are shown in Table 1 and is witnessed that the solutions are in very good agreement for all the considered values of parameters.

5. Results and discussion

The hydromagnetic boundary layer flow and heat transfer of a viscous fluid embedded with suspended dust particles through a non-Darcy porous medium have been investigated. The impacts of viscous dissipation, thermal radiation and non-uniform heat source/sink are considered. Suitable similarity transformations are used to convert the governing time-dependent non-linear boundary layer equations into a system of non-linear ordinary differential equations. Resultant non-linear ordinary differential equations are then solved numerically. In order to have physical insight of the problem, a parametric study has been conducted for different values of the magnetic parameter (M^2), mass concentration of dust particles (l), fluid–particle interaction parameter (β_v), suction/injection parameter (f_0), inertia parameter (α), porous parameter (k_0), Prandtl number (Pr), Eckert number (Ec), heat source/sink parameter ($A^*\&B^*$), unsteadiness parameter (S) and radiation parameter (R) on different flow fields.

Fig. 2 is plotted to demonstrate the comparison between velocity profiles of viscous fluid and dusty viscous fluid. The dust particles mass concentration parameter measures the mass and number of dust particles per unit volume in the flow system. So that, the value $l = 0$ corresponds to clean viscous fluid. It is observed from this plot that, the velocity of dusty viscous fluid is smaller than that of ordinary viscous fluid. This is due to the fact that, the presence of dust particles in clean fluid generates the internal friction within the fluid, consequently, the fluid flow retards. It is also elucidate that, steady flow velocity profiles are higher than that of unsteady state. The dimensionless velocity profiles for different values of magnetic parameter is presented in Fig. 3. It is clearly observed that, the horizontal velocity profile decreased with an increase in magnetic parameter. Further, the momentum boundary layer thickness decreases as M^2 increases and hence induces an increase in the absolute value of the velocity gradient at the surface. The central reason for this is an application of a magnetic field normal to an electrically-conducting fluid has the tendency to produce a drag-like force called the Lorentz force. Which acts in the opposite direction to the flow, as a result, the momentum boundary layer become steeper.

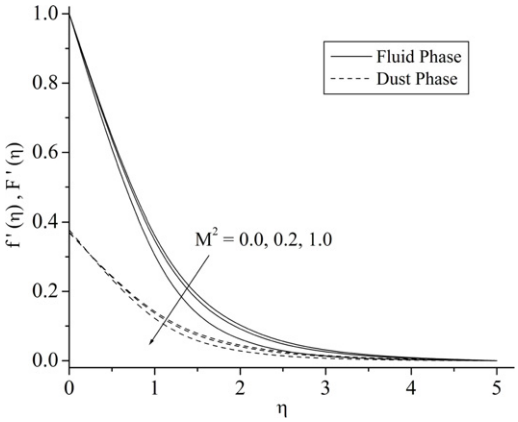

Fig. 3. Effect of M^2 on velocity.

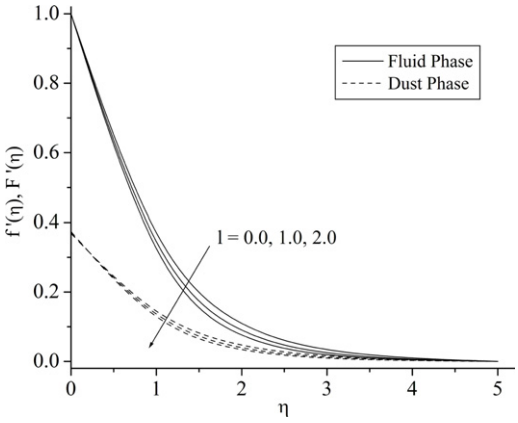

Fig. 4. Effect of l on velocity.

Figs. 4 and 5, are respectively, illustrates the effects of dust particles mass concentration parameter and fluid–particle interaction parameter on the fluid and particle velocity profiles. From Fig. 4 it is observed that, by increasing l the velocity profile is decreases for both phases. Whereas, Fig. 5 illustrate that, an increase in fluid–particle interaction parameter cause increase in particle phase velocity and opposite trend is seen for fluid phase. The effect of the unsteadiness parameter S on the velocity distributions for both phases as a function of η is shown as in Fig. 6. It is interesting to note that the velocity profiles decreases with an increase in the unsteadiness parameter. It is also depict that, the velocity field is higher in the case of steady state flow than that of transient flow.

The influence of blowing ($f_0 < 0$) and suction ($f_0 > 0$) on dimensionless velocity for both phases is as shown in Fig. 7. As expected the opposite results are found for suction and blowing. The blowing or injection causes an increase in fluid velocity profile, whereas by increasing suction ($f_0 > 0$) the fluid velocity profile decreases rapidly near the boundary. Physically this is because, when stronger blowing is provided, the heated fluid is pushed greater extent from the wall, where due to less effect of the viscosity, the flow is accelerated. This effect acts to increase maximum velocity within in the boundary layer. The same principle operates but in opposite direction in case of suction. The Figs. 8 and 9 exhibits the effects of porous parameter and inertia co-efficient of porous medium parameter on both fluid and particle velocity profiles respectively. It is seen from the Fig. 8 that, the velocity profile significantly decreases with an increase in the porous parameter. By this we mean that, the presence of porous medium increases the resistive force in fluid motion, as a result, the velocity field decreases rapidly in the boundary layer. Similar effect has been observed for the effect of inertia co-efficient parameter on velocity profiles as shown in Fig. 9.

Fig. 10 depicts the variation of fluid temperature profile against η for different fluids namely viscous fluid and dusty viscous fluid in the presence and absence of thermal radiation effect. It is observed from this figure that, the thermal boundary layer thickness is higher for ordinary viscous fluid as compared with that of dusty fluid. This due to the fact

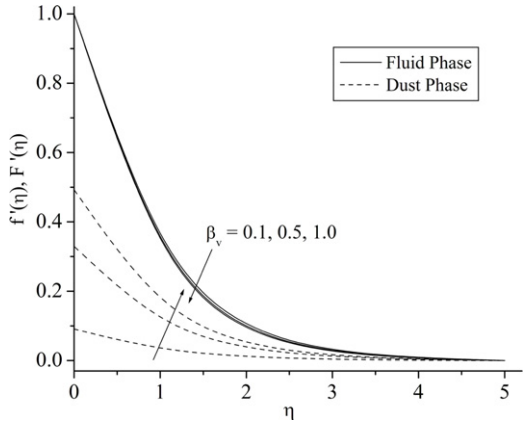

Fig. 5. Effect of β_v on velocity.

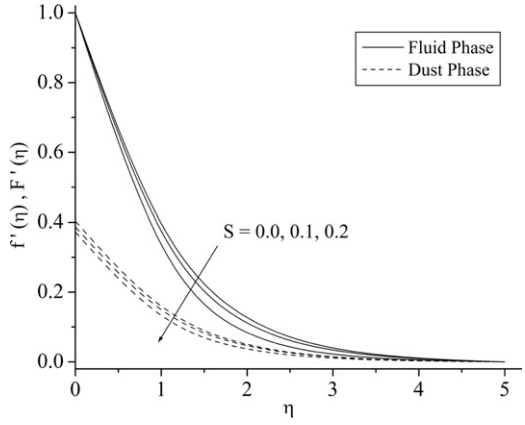

Fig. 6. Effect of S on velocity.

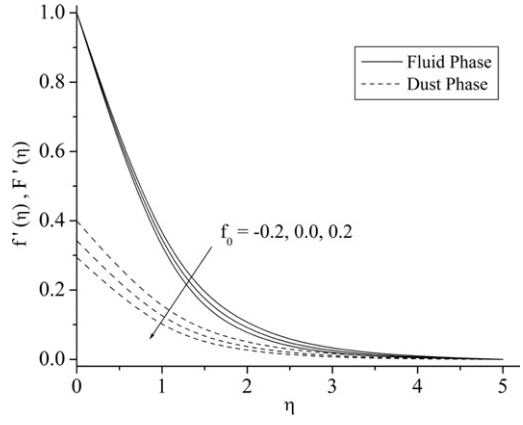

Fig. 7. Effect of f_0 on velocity.

that, the presence of suspended dust particles tends to absorb the heat when they come in contact with the ordinary fluid and this causes a decrease in the fluid temperature. Thus, the dusty viscous fluid plays remarkable role in cooling process than ordinary viscous fluids. From this figure we also note that, the temperature is very high at the porous boundary and asymptotically decreases to zero as $\eta \to \infty$, satisfying the boundary condition. Further, it is observed that, the presence of thermal radiation effect cause an increase in temperature distribution.

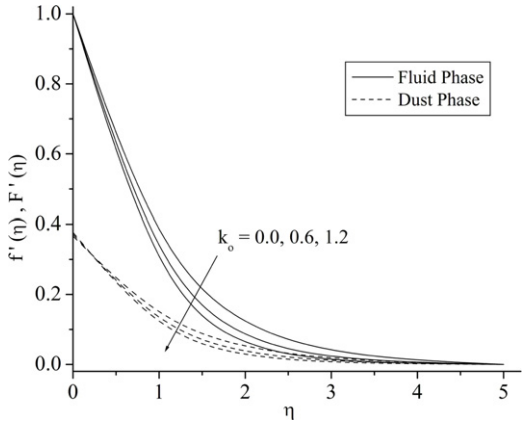

Fig. 8. Effect of k_0 on velocity.

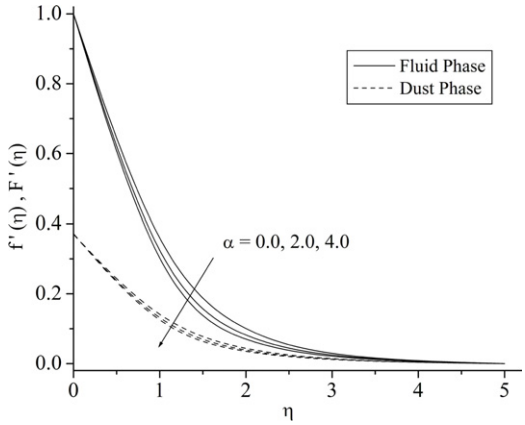

Fig. 9. Effect of α on velocity.

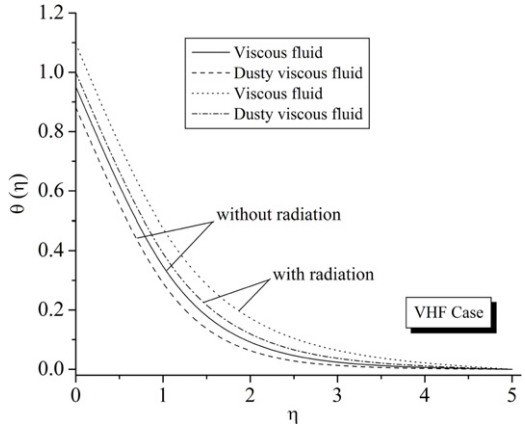

Fig. 10. Temperature for different fluids in VHF case.

Figs. 11–12, are respectively, plotted to depicts the effect of magnetic parameter and dust particles mass concentration parameter on both fluid and particles temperature distributions in VWT and VHF cases. It is observed from the Fig. 11 that, an increase in the values of M^2 have a tendency to increase temperature profile and its associated thermal boundary layer thickness due to the Lorentz force. An opposite phenomenon is observed for the effect of dust

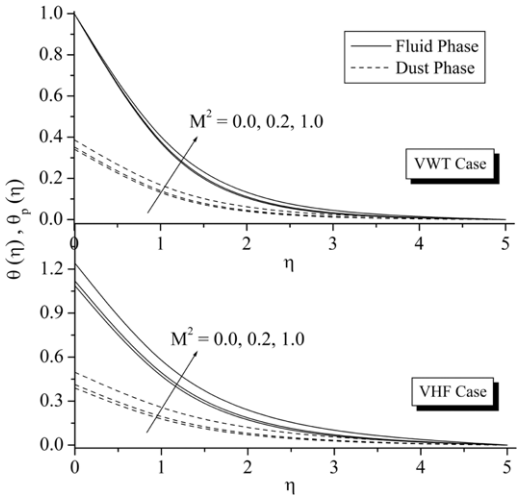

Fig. 11. Effect of M^2 on temperature in VWT and VHF case respectively.

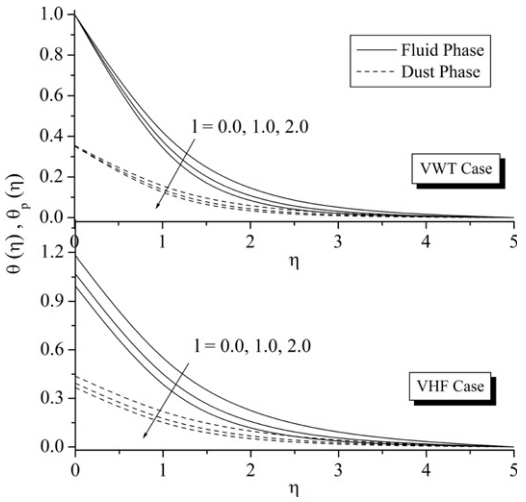

Fig. 12. Effect of l on temperature in VWT and VHF case.

particles mass concentration parameter which is as shown in Fig. 12. The Fig. 13 shows that, the temperature profile for the different values of f_0 in VWT and VHF cases. It is seen that, the temperature profile decreases for increase in f_0. Further, the opposite behavior is observed for suction and injection effect. The heat transfer rate at the surface is higher for suction as compared to injection. This is due to the fact that, the surface shear stress increases when suction is introduced, which in turn increase in the Nusselt number.

The influence of porous parameter and inertia parameter on the temperature distributions for both phases in VWT and VHF cases are respectively presented in Figs. 14 and 15. The Fig. 14 portrays that, when porous parameter increases then the temperature and its associated boundary layer thickens. Which corresponds to decrease in heat transfer rate at the surface. In Fig. 15, the same phenomenon have been observed for the effect of inertia parameter. From Fig. 16 it is seen that, the temperature profile decreases significantly with η in the absence of unsteadiness parameter $S = 0.0$, whereas the temperature profile decreases with an increase in S. By this we can conclude that, the rate of cooling is much faster for higher values of unsteadiness parameter, whereas, it may take longer time for cooling during steady flows. The Fig. 17 presents the effect of increase in Prandtl number on both fluid and particle temperature profiles in VWT and VHF cases. The temperature profile of both the phase is decreased gradually, with an increase in Prandtl number. This is because, the higher Prandtl number fluid has a relatively low thermal conductivity,

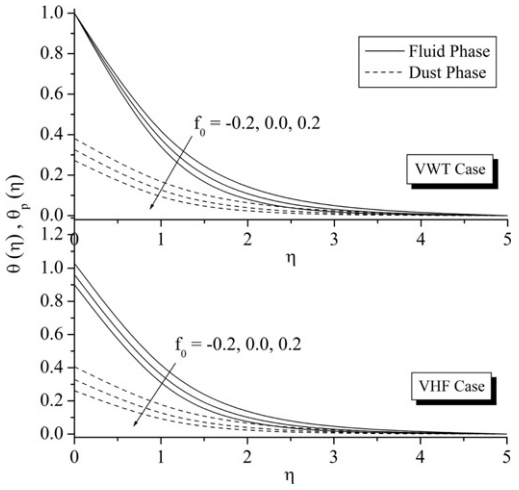

Fig. 13. Effect of f_0 on temperature VWT and VHF case.

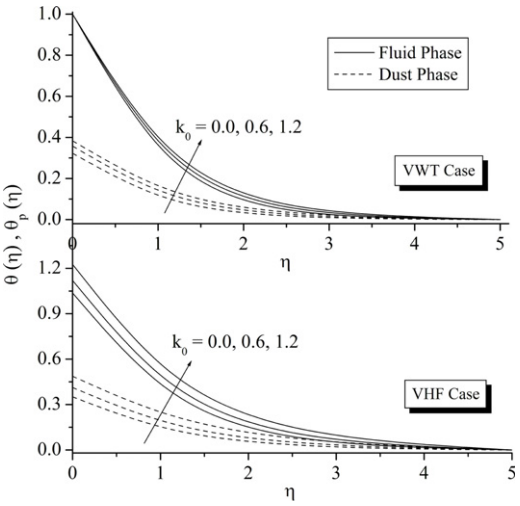

Fig. 14. Effect of k_0 on temperature in VWT and VHF case.

which reduces conduction, and also the thermal boundary layer thickness, and as a consequence it increases the heat transfer rate at the surface.

The effect of space-dependent heat source/sink parameter A^* and temperature-dependent heat source/sink parameter B^* on the horizontal temperature profiles in VWT and VHF cases, are respectively demonstrated as in Figs. 18 and 19 respectively. It is important to mention that $A^* > 0$, $B^* > 0$ corresponds to internal heat generation and $A^* < 0$, $B^* < 0$ corresponds to internal heat absorption. It is the cumulative influence of the space-dependent and temperature-dependent heat source/sink parameter that determines the extent to which the temperature falls or rises in the boundary layer region. From these plots it is clear that, the energy is released for increasing values of $A^* > 0$, $B^* > 0$ and this causes the magnitude of temperature to increase both in VWT and VHF cases, where as energy is absorbed for increasing values of $A^* < 0$, $B^* < 0$ resulting in temperature dropping significantly near the boundary layer. Further, the thermal boundary layer thicker for heat source effect than that of heat sink effect. In Fig. 20 the effects of thermal radiation on temperature field for both phase is shown in VWT and VHF cases. In this case, the temperature field increases with an increase in thermal radiation parameter. Further, it depicts that, the thermal boundary layer thickness is higher in the presence of thermal radiation effect ($R \neq 0$) than in its absence (i.e., $R = 0$). The same behavior is observed for the effect of Eckert number on temperature profile as shown in the

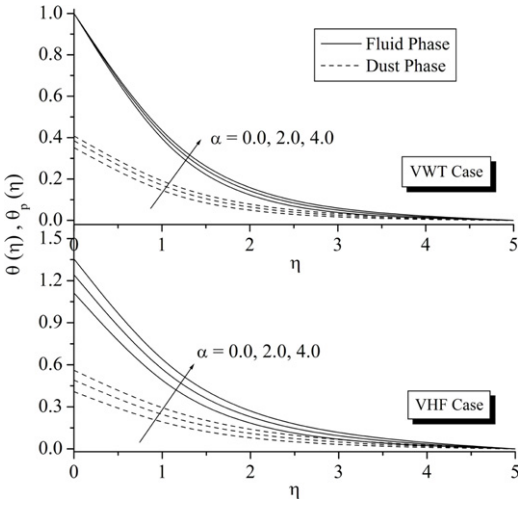

Fig. 15. Effect of α on temperature in VWT and VHF case.

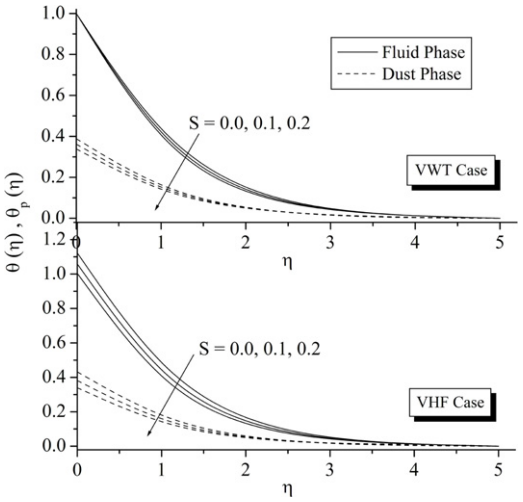

Fig. 16. Effect of S on temperature in VWT and VHF case.

Fig. 21. This is because, the viscous dissipation transforms the kinetic energy of the fluid into internal energy of the fluid, which cause loss of heat from the sheet to the fluid i.e., heating up of the fluid.

Finally, the variation of skin friction coefficient and Nusselt number profiles for different values of M^2, Ec, β_v, l, k_0, α, R, A^* and B^* are presented in Table 2. It is seen that, the skin friction co-efficient at the surface ($f''(0)$) is decreases for increasing values of M^2, α, k_0, l and β_v. There is no variation occurs for the effects of R, A^*, B^* and Ec. Further, the rate of heat transfer at the surface increases with an increase in dust particles mass concentration parameters. While this phenomenon is opposite for the effect of increasing values of M^2, Ec, β_v, k_0, α and A^*. Additionally, it is observed that, the wall temperature increases for increasing values of M^2, Ec, β_v, k_0, α and A^*. It is worth mentioning that, the fluid phase velocity and temperature fields are parallel, and fluid phase velocity and temperature fields are higher than that of dust phase velocity and temperature fields. In addition, the VHF case temperature fields are higher than that of VWT case temperature fields.

6. Concluding remarks

Theoretical analysis of hydromagnetic boundary layer flow and heat transfer over an unsteady permeable stretching surface though a non-Darcy porous medium in dusty viscous fluid has been investigated. Momentum boundary

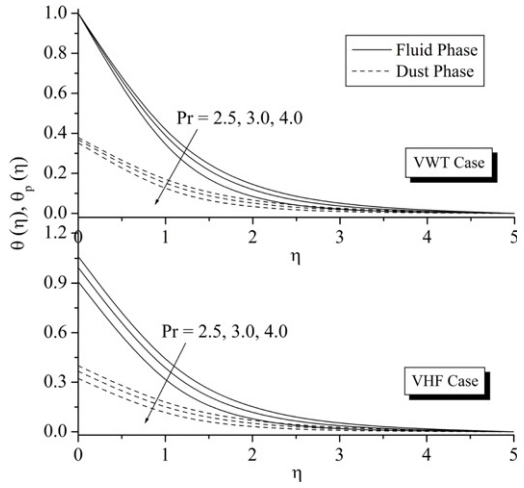

Fig. 17. Effect of *Pr* on temperature in VWT and VHF case.

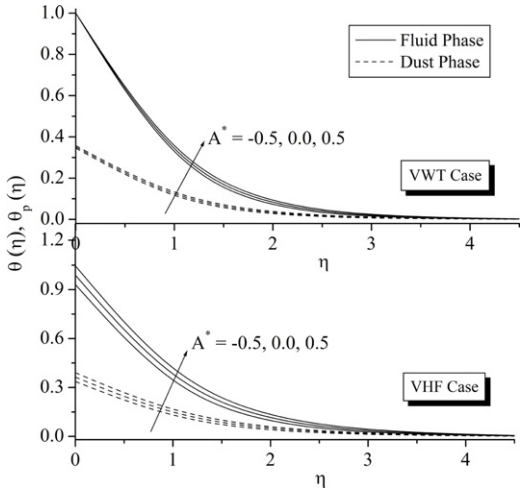

Fig. 18. Effect of A^* on temperature in VWT and VHF case.

layer includes the effect of variable transverse magnetic field and non-Darcy porous medium. Whereas, the thermal boundary layer equation includes the effect of thermal radiation, non-uniform heat source/sink and viscous dissipation. The governing partial differential equations are reduced into a set of non-linear ordinary differential equations by means of suitable similarity transformations. Reduced system of coupled non-linear ordinary differential equations are numerically solved using an efficient Fehlberg fourth–fifth order Runge–Kutta method. The important conclusions are summarized as follows.

- The momentum boundary layer is thinner for the effect of dust particles mass concentration parameter, magnetic parameter, porous parameter, inertia parameter and unsteady parameter.
- The blowing causes an increase in fluid and particle velocity profile whereas opposite effect is seen in case of suction.
- For effective cooling of the stretching sheet, space and temperature-dependent heat sinks are desirable.
- Thermal boundary layer is thinner for the effect of blowing than that of suction effect.
- The effect of Prandtl number is to decrease the thermal boundary layer thickness and this manner is opposite for the effect of porous parameter, magnetic parameter and Eckert number.
- In arriving at an appropriate polymer extrusion it is desirable that the operating temperatures are as low as possible to ensure minimum thermal radiation effect.

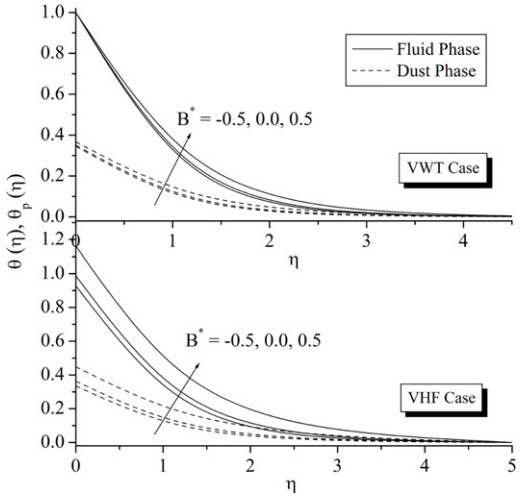

Fig. 19. Effect of B^* on temperature in VWT and VHF case.

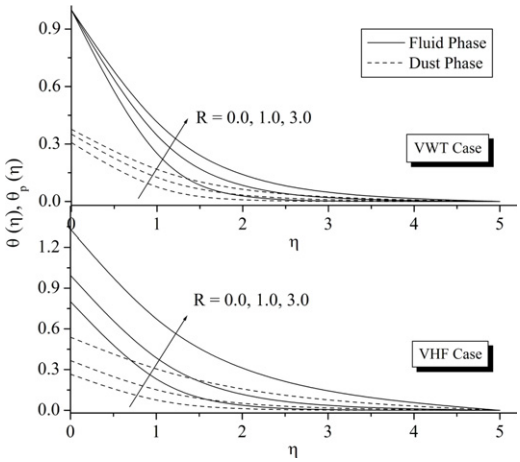

Fig. 20. Effect of R on temperature in VWT and VHF case.

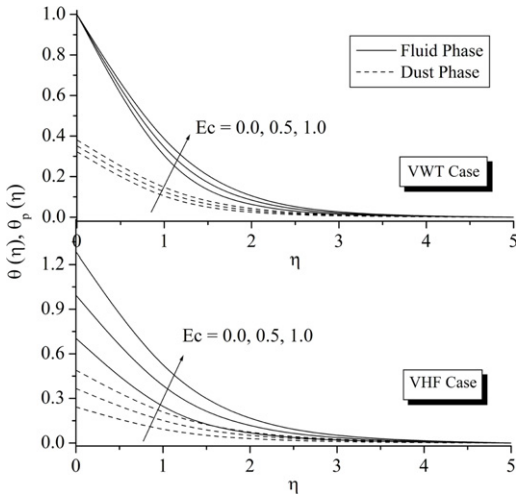

Fig. 21. Effect of Ec on temperature in VWT and VHF case.

Table 2
Numerical values of $f''(0)$, $-\theta'(0)$ and $\theta(0)$ for different values of M^2, Ec, β_v, l, k_0, α, R, A^* and B^*.

M^2	Ec	β_v	l	k_0	α	R	A^*	B^*	$f''(0)$	$-\theta'(0)$ VWT	$\theta(0)$ VHF
0.0	0.5	0.5	0.5	0.4	0.1	0.5	0.05	0.05	−1.24252	0.98809	1.00864
0.2									−1.31478	0.94241	1.04233
0.6									−1.44917	0.85706	1.10753
0.4	0.0	0.5	0.5	0.4	0.1	0.5	0.05	0.05	−1.38350	1.33241	0.75271
	0.2								−1.38350	−0.40203	2.04296
	0.3								−1.38350	−1.26925	2.68809
0.4	0.5	1	0.5	0.4	0.1	0.5	0.05	0.05	−1.40150	0.88845	1.08319
		1.5							−1.41537	0.88285	1.08751
		2							−1.42438	0.88035	1.08948
0.4	0.5	0.5	0	0.4	0.1	0.5	0.05	0.05	−1.32355	0.83209	1.13527
			0.5						−1.38350	0.89880	1.07527
			1						−1.44052	0.96037	1.02752
0.4	0.5	0.5	0.5	0	0.1	0.5	0.05	0.05	−1.24252	0.98809	1.00864
				0.3					−1.34955	0.92036	1.05889
				0.6					−1.44917	0.85706	1.10753
0.4	0.5	0.5	0.5	0.4	0	0.5	0.05	0.05	−1.36083	0.90872	1.06772
					0.5				−1.47100	0.86038	1.10488
					1				−1.57407	0.81488	1.14066
0.4	0.5	0.5	0.5	0.4	0.1	0	0.05	0.05	−1.38350	1.09424	0.94627
						1			−1.38350	0.77826	1.19837
						2			−1.38350	0.63320	1.42383
0.4	0.5	0.5	0.5	0.4	0.1	0.5	−1	0.05	−1.38350	1.14773	0.89010
							0		−1.38350	0.91065	1.06646
							1		−1.38350	0.67358	1.24282

- Dusty viscous fluid is favorable for cooling processes than ordinary viscous fluid.
- The prescribed heat flux boundary condition is better suited for effective cooling of the stretching sheet.
- The Rate of heat transfer at the wall are suppresses with increase in inertia parameter.
- The Momentum and thermal boundary layer are thinner due to the influence of suspended dust particles.
- If $l = M^2 = k_0 = \alpha = f_0 = A^* = B^* = R = Ec = 0$ and $S = 0$, then our results coincides with the results of Grubka and Bobba [3], Ishak et al. [14,15] and El-Aziz [17] for limiting cases.

Acknowledgments

The authors wish to express their deep sense of gratitude to the reviewers of the original manuscript for their kind suggestions based upon which the present version of the paper has been prepared. The author B.J. Gireesha wishes to express his gratitude to University Grants Commission (No. F 5-110/2014 (IC)), New Delhi, India for the financial support under Raman Fellowship 2014–2015 for pursuing this work.

References

[1] Sakiadis BC. Boundary layer behaviour on continuous solid surface. AIChE J 1961;7:26–8.
[2] Tsou FK, Sparrow EM, Goldstein RJ. Flow and heat transfer in the boundary layer on a continuous moving surface. Int J Heat Mass Transfer 1967;10:219–35.
[3] Grubka LJ, Bobba KM. Heat transfer characteristics of a continuous stretching surface with variable temperature. ASME J Heat Transfer 1985;107:248–50.
[4] Akbar NS, Khan ZH, Nadeem S. The combined effects of slip and convective boundary condition on stagnation-point flow of CNT suspended nanofluid over a stretching sheet. J Mol Liq 2014;196:21–5.
[5] Starov VM, Zhdanov VG. Effective viscosity and permeability of porous media. Colloids Surf A 2001;192:363–75.
[6] Kiwan S, Ali ME. Near-slit effects on the flow and heat transfer from a stretching plate in a porous medium. Numer Heat Transfer A 2008; 54:93–108.

[7] Gireesha BJ, Mahanthesh B, Rashidi MM. MHD boundary layer heat and mass transfer of a chemically reacting Casson fluid over a permeable stretching surface with non-uniform heat source/sink. Int J Ind Math 2015;7:14.
[8] Tamayol A, Hooman K, Bahrami M. Thermal analysis of flow in a porous medium over a permeable stretching wall. Transport Porous Med 2010;8:661–76.
[9] Hong JT, Yamada Y, Tien CL. Effect of non-Darcian and nonuniform porosity on vertical plate natural convection in porous medium. Int J Heat Mass Transfer 1987;109:356–62.
[10] Mohammadein AA, El-Amin MF. Thermal dispersion-radiation effects on non-Darcy natural convection in a fluid saturated porous medium. Transport Porous Med 2000;40(2):153–63.
[11] Khani F, Farmany A, Ahmadzadeh M, Aziz A, Samadi F. Analytic solution for heat transfer of a third grade viscoelastic fluid in non-Darcy porous media with thermophysical effects. Commun Nonlinear Sci Numer Simul 2009;14:3867–78.
[12] Pal D, Chatterjee S. Heat and mass transfer in MHD non-Darcian flow of a micropolar fluid over a stretching sheet embedded in a porous media with non-uniform heat source and thermal radiation. Commun Nonlinear Sci Numer Simul 2010;15:1843–57.
[13] Chen CH. Heat transfer in a power-law fluid film over a unsteady stretching sheet. Heat Mass Transfer 2003;39:791–6.
[14] Ishak A, Nazar R, Pop I. Boundary layer flow and heat transfer over an unsteady stretching vertical surface. Meccanica 2009;44:369–75.
[15] Ishak A, Nazar R, Pop I. Mixed convection on the stagnation point flow towards a vertical continuously stretching sheet. ASME J Heat Transfer 2007;129:1087–90.
[16] Abel MS, Mahesha N, Tawade J. Heat transfer in a liquid film over an unsteady stretching surface with viscous dissipation in presence of external magnetic field. Appl Math Model 2009;33:3430–41.
[17] Aziz MA. Mixed convection flow of a micropolar fluid from an unsteady stretching surface with viscous dissipation. J Egyptian Math Soc 2013;21:385–94.
[18] Pal D, Mondal H. Hydromagnetic non-Darcy flow and heat transfer over a stretching sheet in the presence of thermal radiation and Ohmic dissipation. Commun Nonlinear Sci Numer Simul 2010;15:1197–209.
[19] Cortell R. Combined effect of viscous dissipation and thermal radiation on fluid flows over a non-linearly stretched permeable wall. Meccanica 2012;47:769–81.
[20] Motsumi TG, Makinde OD. Effects of thermal radiation and viscous dissipation on boundary layer flow of nanofluids over a permeable moving flat plate. Phys Scr 2012;86:1–8.
[21] Akbar NS, Nadeem S, Ul Haq R, Khan ZH. Radiation effects on MHD stagnation point flow of nano fluid towards a stretching surface with convective boundary condition. Chin J Aeronaut 2013;26:1389–97.
[22] Mahantesh MN, Abel MS, Vajravelu K. Flow and heat transfer characteristics of viscoelastic fluid in a porous medium over an impermeable stretching sheet with viscous dissipation. Int J Heat Mass Transfer 2010;53:4707–13.
[23] Liu IC, Wang HH, Umavathi JC. Effect of viscous dissipation internal heat source/sink, and thermal radiation on a hydromagnetic liquid film over an unsteady stretching sheet. ASME J. Heat Transfer 2013;135:031701–31706.
[24] Saffman PG. On the stability of laminar flow of a dusty gas. J Fluid Mech 1962;13:120–8.
[25] Datta N, Mishra SK. Boundary layer flow of a dusty fluid over a semi-infinite flat plate. Acta Mech 1982;42:71–83.
[26] Vajravelu K, Nayfeh J. Hydromagnetic flow of a dusty fluid over a stretching sheet. Int J Nonlinear Mech 1992;27:937–45.
[27] Makinde OD, Chiyoka T. MHD transient flows and heat transfer of dusty fluid in a channel with variable physical properties and Navies slip condition. Comput Math Appl 2010;60:660–9.
[28] Nandkeolyar R, Seth GS, Makinde OD, Sibanda P, Ansari MS. Unsteady hydromagnetic natural convection flow of a dusty fluid past an impulsively moving vertical plate with ramped temperature in the presence of thermal radiation. ASME J Appl Mech 2013;680:9. http://dx.doi.org/10.1115/1.4023959.
[29] Gireesha BJ, Ramesh GK, Abel MS, Bagewadi CS. Boundary layer flow and heat transfer of a dusty fluid over a stretching sheet with non-uniform heat source/sink. Int J Multiph Flow 2011;37:977–82.
[30] Gireesha BJ, Roopa GS, Bagewadi CS. Effect of viscous dissipation and heat source on flow and heat transfer of a dusty fluid over unsteady stretching sheet. Appl Math Mech (English Ed) 2012;30(8):1001–14.
[31] Gireesha BJ, Mahanthesh B, Gorla RSR. Suspended particle effect on nanofluid boundary layer flow past a stretching surface. J Nanofluid 2014;3:267–77.
[32] Gireesha BJ, Mahanthesh B, Gorla RSR, Manjunath PT. Thermal radiation and Hall effects on boundary layer flow past a non-isothermal stretching surface embedded in porous medium with non-uniform heat source/sink and fluid-particle suspension. Heat Mass Transfer 2015; http://dx.doi.org/10.1007/s00231-015-1606-3.
[33] Abramowitz M, Stegun IA. Hand book of mathematical functions. New York: Dover; 1965.